

# Early Universe Tomography with CMB and Gravitational Waves

Sachiko Kuroyanagi\*

*Research Center for the Early Universe, University of Tokyo, Tokyo 113-0033, Japan*

Christophe Ringeval†

*Centre for Cosmology, Particle Physics and Phenomenology,  
Institute of Mathematics and Physics, Louvain University,  
2 Chemin du Cyclotron, 1348 Louvain-la-Neuve, Belgium*

Tomo Takahashi‡

*Department of Physics, Saga University, Saga 840-8502, Japan*  
(Dated: June 27, 2018)

We discuss how one can reconstruct the thermal history of the Universe by combining cosmic microwave background (CMB) measurements and gravitational wave (GW) direct detection experiments. Assuming various expansion eras to take place after the inflationary reheating and before Big-Bang Nucleosynthesis (BBN), we show how measurements of the GW spectrum can be used to break the degeneracies associated with CMB data, the latter being sensitive to the total amount of cosmic expansion only. In this context, we argue that the expected constraints from future CMB and GW experiments can probe a scenario in which there exists late-time entropy production in addition to the standard reheating. We show that, for some cases, combining data from future CMB and GW direct detection experiments allows the determination of the reheating temperature, the amount of entropy produced and the temperature at which the standard radiation era started.

PACS numbers: 98.80.Cq, 98.70.Vc

## I. INTRODUCTION

Our understanding of the evolution of the Universe is now becoming clearer owing to precise cosmological observations such as cosmic microwave background, large scale structure (LSS), type Ia supernovae and others. From such observations, we can obtain information about the current energy budget and the history of the Universe. In particular, the evolution after the time of Big-Bang Nucleosynthesis to the present is relatively well understood. On the other hand, one can also probe the evolution during inflation since cosmic density fluctuations, which can be probed by CMB and LSS, are considered to be initially generated during that epoch.

Compared to the the above mentioned eras, the evolution, or thermal history of the Universe during the period after inflation to BBN is relatively unexplored, certainly due to the lack of associated cosmological observables. Although, in the standard scenario, the Universe is considered to be radiation-dominated until BBN (precisely speaking, until the radiation-matter equality epoch) after the inflaton reheating, the thermal history can be more complicated. In theories beyond the standard model of particle physics such as in supersymmetric models and string theory, there can exist some scalar fields (other than the inflaton, as for instance moduli field) that are

long-lived and can dominate the energy density of the Universe. Their decay may also produce huge amount of entropy thereby influencing the early universe history.

In the light of these considerations, it would be worth investigating how one could probe the thermal history during these epochs. In fact, some authors have investigated this issue by using observations of CMB [1–3] and direct detection of gravitational waves (GW) in Refs. [4–7], while using the combination of both has been pushed forward in Ref. [8]. From CMB observations, we can probe the amplitude of the primordial scalar and tensor fluctuations as well as their scale dependencies around the so-called pivot scale. Notice that the time at which such a reference scale exited the Hubble radius during inflation depends on the amount of cosmic expansion from Hubble exit to the present times, which of course includes all of the above-mentioned post-inflationary eras. As a result, by measuring the primordial power spectra in a given inflationary model, we can obtain information on the amount of the total cosmic expansion, i.e. the integrated thermal history since the end of inflation. This can be also applicable in GW direct detection experiments through measurements of the amplitude and scale dependence of tensor fluctuations. Not only that, direct detection of GWs could be used to probe the background evolution as the shape of the GW’s spectrum is very sensitive to it. Thus, in the inflationary framework, detection/non-detection of GWs can give invaluable information on the thermal history of the Universe thereby allowing a “tomography” of these eras.

In this paper, we investigate this issue by complementing observations of the CMB and GWs, paying particular

\*Electronic address: skuro@resceu.s.u-tokyo.ac.jp

†Electronic address: christophe.ringeval@uclouvain.be

‡Electronic address: tomot@cc.saga-u.ac.jp

attention to the period from the end of inflation to BBN. For this purpose, we first recall how one can constrain the thermal history of the Universe from these experiments. Although we have not detected any gravitational waves yet, CMB observations, such as those from the Wilkinson Microwave Anisotropy Probe (WMAP) [9], are precise enough to already give some constraints within some inflationary models [3]. However, in the near future, a direct detection of GWs could be achieved for some inflationary models that would allow to combine both CMB and GWs experiments. To see this in an explicit manner, we investigate the projected constraints on the thermal history of the Universe from future observations of CMB such as CMBpol and the PLANCK satellite combined with future direct detection GW experiments such as BBO [10], DECIGO [11] and Ultimate-DECIGO [12].

The organization of this paper is as follows. In the next section, we give a brief description on how CMB and GWs can probe or constrain the thermal history after inflation and justify their complementarity. We also give the current constraints on the thermal history within the so-called large field model of inflation coming from CMB using WMAP data. Then in Section III, we present our forecasts derived from a Fisher matrix analysis based on the above-mentioned future CMB and GWs experiments. We conclude in the last section.

## II. CMB AND GWS AS A PROBE OF THE THERMAL HISTORY OF THE UNIVERSE

In this section, we describe how one can probe the thermal history of the Universe with CMB and GW observations in the context of inflationary cosmology.

We assume that inflation is the origin of both scalar and tensor perturbations around the Friedmann–Lemaître–Robertson–Walker (FLRW) metric

$$ds^2 = -a^2(1 + 2\Phi)d\eta^2 + a^2[(1 - 2\Psi)\delta_{ij} + h_{ij}]dx^i dx^j, \quad (1)$$

where  $\Psi$  and  $\Phi$  are the Bardeen potential and  $h_{ij}$  is the transverse and traceless spin two fluctuations. If inflation is driven by a slowly-rolling scalar field  $\phi$ , the quantum fluctuations of the field–metric system generate an almost scale invariant power spectrum for both kinds of perturbation. The observable quantities are those which are conserved on super-Hubble scales, that is the comoving curvature for scalar perturbations, which reads in the longitudinal gauge,

$$\zeta(\eta, \mathbf{x}) \equiv \Psi(\eta, \mathbf{x}) + \mathcal{H} \frac{\delta\phi(\eta, \mathbf{x})}{\phi'}, \quad (2)$$

where  $\mathcal{H} \equiv aH$  is the conformal Hubble parameter and a prime denotes derivatives with respect to the conformal time  $\eta$ . The tensor modes  $h_{ij}$  are themselves gauge invariant and conserved on super-Hubble scales. It is convenient to decompose them on their two polarization

states  $h_\lambda$  in Fourier space as

$$h_{ij}(\eta, \mathbf{x}) = \sum_{\lambda=+, \times} \int \frac{dk^3}{(2\pi)^{3/2}} h_\lambda(\eta, \mathbf{k}) \varepsilon_{ij}^\lambda e^{i\mathbf{k} \cdot \mathbf{x}}, \quad (3)$$

where  $\varepsilon_{ij}^\lambda$  are the polarization tensors satisfying  $\varepsilon_{ij}^\lambda \varepsilon_{\lambda'}^{ij} = 2\delta_{\lambda\lambda'}$ .

At first order in the slow-roll formalism, the primordial power spectrum for the scalars is given by [13]

$$\mathcal{P}_\zeta \equiv \frac{k^3}{2\pi^2} |\zeta|^2 \simeq \frac{H_*^2}{8\pi^2 M_{\text{pl}}^2 \epsilon_{1*}} \times \left[ 1 - 2(C + 1)\epsilon_{1*} - C\epsilon_{2*} - (2\epsilon_{1*} + \epsilon_{2*}) \ln \frac{k}{k_*} \right], \quad (4)$$

while the tensor spectrum (sum of polarization included) reads

$$\mathcal{P}_h \equiv \frac{2k^3}{\pi^2} |h|^2 \simeq \frac{2H_*^2}{\pi^2 M_{\text{pl}}^2} \left[ 1 - 2(C + 1)\epsilon_{1*} - 2\epsilon_{1*} \ln \frac{k}{k_*} \right]. \quad (5)$$

In these equations,  $M_{\text{pl}}^2 = 1/(8\pi G)$  stands for the reduced Planck mass,  $C = -2 + \ln 2 + \gamma_E \simeq 0.73$  with  $\gamma_E$  being the Euler constant and  $\epsilon_i$  are the slow-roll parameters which are defined as<sup>1</sup>

$$\epsilon_1 \equiv -\frac{d \ln H}{dN}, \quad \epsilon_2 \equiv \frac{d \ln \epsilon_1}{dN}, \quad (8)$$

where  $N \equiv \ln a$  is the number of  $e$ -folds. The spectral index defined as  $n_s - 1 = d \ln \mathcal{P}_\zeta / d \ln k$  is given by

$$n_s = 1 - 2\epsilon_{1*} - \epsilon_{2*}. \quad (9)$$

The tensor-to-scalar ratio  $r$ , which is usually used to quantify the amplitude of the tensor mode, is given by

$$r \equiv \frac{\mathcal{P}_h}{\mathcal{P}_\zeta} = 16\epsilon_{1*}. \quad (10)$$

An asterisk “\*” indicates that the quantities have to be evaluated at the time when the pivot mode  $k_*$  crossed the Hubble radius during inflation, i.e. the solution of

$$k_* = a(\eta_*)H(\eta_*). \quad (11)$$

<sup>1</sup> In the literature, the slow-roll parameters defined using the potential for the inflaton  $V(\phi)$  are also used, which are given by  $\epsilon_V = (1/2)M_{\text{pl}}^2 (V'/V)^2$  and  $\eta_V = M_{\text{pl}}^2 (V''/V)$  with a prime representing the derivative with respect to  $\phi$ . The correspondence between  $\{\epsilon_V, \eta_V\}$  and  $\{\epsilon_1, \epsilon_2\}$  at leading order in slow-roll parameters are :

$$\epsilon_1 = \epsilon_V, \quad \epsilon_2 = 2\epsilon_V - 2\eta_V. \quad (6)$$

With these parameters, the spectral index and the tensor-to-scalar ratio are respectively given by

$$n_s = 1 - 6\epsilon_{V*} + 2\eta_{V*}, \quad r = 16\epsilon_{V*}. \quad (7)$$

Here, we neglect the running of the spectral index, which will not affect our results for CMB. However, we note that such truncation can give large deviation for the power spectrum from the one obtained exact numerical calculation in some models [14].

### A. CMB constraints on the post-inflationary universe history

#### 1. Standard scenario

The power spectrum functional forms of Eqs. (4) and (5) are usually compared to the current CMB data to constrain the slow-roll (Hubble flow) parameters, or equivalently the spectral index and tensor-to-scalar ratio [1, 9, 15–20]. This is done by choosing a pivot scale  $k_*$  in the observable range, typically  $k_* = 0.05 \text{ Mpc}^{-1}$ . However, if one assumes an inflationary model, there is much more to say. Indeed, the tensor-to-scalar ratio, the spectral index and all other observable quantities are completely determined by the inflaton potential  $V(\phi)$ . As discussed earlier, they have to be evaluated at the time  $\eta_*$ , which can be determined by solving Eq. (11). In order to obtain  $\eta_*$ , it is compulsory to make assumptions on the subsequent thermal history of the universe, i.e. including at least the reheating and preheating stages. In terms of the number of  $e$ -folds during inflation, the physical pivot wavenumber is given by

$$\frac{k_*}{a} = \frac{k_*}{a_0} (1 + z_{\text{end}}) e^{N_{\text{end}} - N}, \quad (12)$$

where  $z_{\text{end}}$  is the redshift at which inflation ended, after  $N_{\text{end}}$   $e$ -folds. As shown in Refs. [1–3, 21], a convenient way to calculate  $z_{\text{end}}$  is to introduce the so-called “reheating parameter”

$$R_{\text{rad}} \equiv \frac{a_{\text{end}}}{a_{\text{reh}}} \left( \frac{\rho_{\text{end}}}{\rho_{\text{reh}}} \right)^{1/4}. \quad (13)$$

The quantity  $R_{\text{rad}}$  encodes all of our ignorance of the subsequent thermal evolution after the end of inflation and quantifies any deviations from a pure radiation era. In fact, by assuming instantaneous transition between the inflationary epoch to inflaton oscillating era and inflaton oscillating to radiation-dominated eras, one has

$$1 + z_{\text{end}} = \frac{1}{R_{\text{rad}}} \left( \frac{\rho_{\text{end}}}{\tilde{\rho}_{\gamma_0}} \right)^{1/4}, \quad (14)$$

where  $\rho_{\text{end}}$  is the energy density of the universe at the end of inflation and  $\tilde{\rho}_{\gamma_0}$  is the energy density of radiation today, eventually rescaled by any change in the number of gravitating relativistic degrees of freedom. In terms of the cosmological parameters today,

$$\tilde{\rho}_{\gamma_0} = \mathcal{Q}_{\text{reh}} \rho_{\gamma_0} = 3 \mathcal{Q}_{\text{reh}} \frac{H_0^2}{M_{\text{pl}}^2} \Omega_{r_0}, \quad (15)$$

where we have defined

$$\mathcal{Q}_{\text{reh}} \equiv \frac{g_{\text{reh}}}{g_0} \left( \frac{g_{s0}}{g_{s\text{reh}}} \right)^{4/3}. \quad (16)$$

Here,  $g_s$  and  $g$  respectively denotes the number of entropic and energetic relativistic degrees of freedom at the epoch of interest.  $H_0$  and  $\Omega_{r_0}$  are the Hubble parameter and radiation density parameter today.

As shown in Ref. [21], using energy conservation, Eq. (13) can be recast into two other strictly equivalent forms

$$\begin{aligned} \ln R_{\text{rad}} &= \frac{1}{4} (N_{\text{reh}} - N_{\text{end}}) (3\bar{w}_{\text{reh}} - 1) \\ &= \frac{1 - 3\bar{w}_{\text{reh}}}{12(1 + \bar{w}_{\text{reh}})} \ln \left( \frac{\rho_{\text{reh}}}{\rho_{\text{end}}} \right), \end{aligned} \quad (17)$$

with  $\bar{w}_{\text{reh}}$  standing for the *mean* equation of state parameter during the inflaton oscillating era. Using  $R_{\text{rad}}$ , Eq. (11) is solved for the  $e$ -fold time  $\Delta N_* \equiv N_* - N_{\text{end}}$ , verifying [21]

$$\begin{aligned} \Delta N_* &= -\ln R_{\text{rad}} + N_0 - \frac{1}{4} \ln \left( \frac{H_*^2}{M_{\text{pl}}^2 \epsilon_{1*}} \right) \\ &\quad + \frac{1}{4} \ln \left( \frac{3}{\epsilon_{1*}} \frac{V_{\text{end}}}{V_*} \frac{3 - \epsilon_{1*}}{3 - \epsilon_{1\text{end}}} \right), \end{aligned} \quad (18)$$

where the constant  $N_0$  stands for

$$N_0 \equiv \ln \left( \frac{k_*/a_0}{\tilde{\rho}_{\gamma_0}^{1/4}} \right). \quad (19)$$

Let us emphasize that the right hand side of Eq. (18) usually depends on  $\Delta N_*$  itself, but in a completely algebraic way once the model, i.e.  $V(\phi)$ , is specified. It can also be simplified further by using  $\epsilon_{1*} \ll 1$ ,  $\epsilon_{1\text{end}} = 1$  and Eq. (4) as,

$$\Delta N_* = -\ln R_{\text{rad}} + N_0 - \frac{1}{4} \ln(8\pi^2 \mathcal{P}_*) - \frac{1}{4} \ln \frac{r}{72} + \frac{1}{4} \ln \frac{V_{\text{end}}}{V_*}. \quad (20)$$

As an example, we have plotted in Fig. 1 the predicted values for  $\epsilon_{1*}$ ,  $\epsilon_{2*}$ , as well as the spectral index  $n_s$  and tensor-to-scalar ratio  $r$  for the chaotic inflation models with  $V(\phi) \propto \phi^p$ . We show the cases of  $p = 1, 2, 3, 4, 6$  and  $10$ . For each  $p$ , there is a range of possible  $\Delta N_*$  since the reheating should occur from the end of inflation to the BBN epoch, whose values are indicated in the figure at both end points and for each case of  $p$ . Along with the theoretical predictions, we also show  $1\sigma$  and  $2\sigma$  confidence intervals associated with the WMAP7 data [3, 22, 23] and Hubble Space Telescope (HST) data [24]. From the figure, one can easily see that inflation models with  $p \geq 3$  are excluded by current data. Even for the cases with  $p = 2$  and  $1$ , there is a lower bound on  $|\Delta N_*|$  to be consistent with WMAP7, which can be translated into the constraints on the thermal history of the Universe.

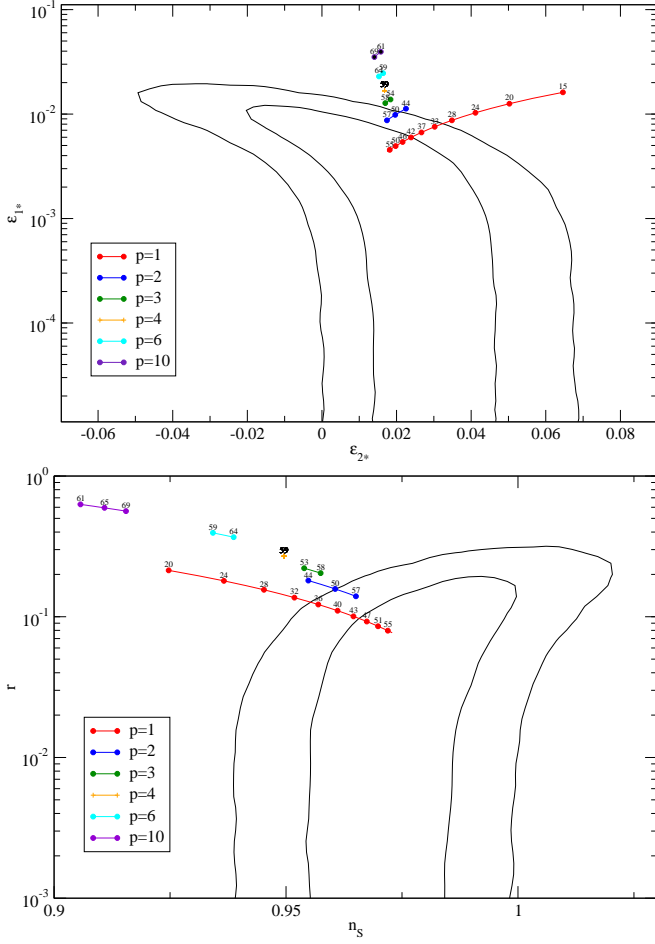


FIG. 1: WMAP7 constraints in the plane  $(\epsilon_{1*}, \epsilon_{2*})$  (top) and  $(n_s, r)$  (bottom) compared with the large field model predictions obtained by solving Eq. (18) for various monomial potentials  $V(\phi) \propto \phi^p$ . The annotated values are those of  $|\Delta N_*|$  and they range for a reheating occurring as low as BBN to an instantaneous reheating after inflation.

## 2. Non-standard scenarios

Up to here, we have assumed the “standard” scenario in which once the reheating from the inflaton is completed, the Universe becomes radiation dominated until the radiation-matter equality  $z_{\text{eq}} \sim 10^4$ . However, this standard scenario could be modified. For instance, if one assumes that, inserted after the reheating era there is a phase of evolution dominated by a gravitating source  $X$ , characterized by an equation of state parameter  $w_x$ . As shown in Ref. [21], one can define a parameter  $R_x$  exactly as in Eq. (13) by

$$R_x \equiv \frac{a_{\text{xini}}}{a_{\text{xend}}} \left( \frac{\rho_{\text{xini}}}{\rho_{\text{xend}}} \right)^{1/4}, \quad (21)$$

for which it is immediate to verify that Eq. (17) also applies using the mean value  $\bar{w}_x$  and by the replacement

“end  $\rightarrow$  xini”, “reh  $\rightarrow$  xend”. From this definition, one can check that all equations are unchanged, and in particular Eq. (18), by replacing  $R_{\text{rad}}$  with  $R_{\text{rad}}R_x$ . Assuming another  $Y$ -era to take place just after the  $X$ -era and before the radiation-dominated era, we would reach exactly the same conclusions by replacing  $R_{\text{rad}}R_x$  with  $R_{\text{rad}}R_xR_y$ . In other words, CMB can only constrain the overall thermal history and only feels those parameters,  $R_{\text{rad}}R_xR_y \dots$ , multiplied. Let us also notice that the correction coefficient entering Eq. (15) is now given by  $\mathcal{Q}_{\text{yend}}$  instead of  $\mathcal{Q}_{\text{reh}}$ .

As a well motivated example, and the one we will be discussing in Sec. III, such a situation is typical of scenarios in which a late-decaying massive scalar field, denoted as  $\sigma$  hereafter, produce a large amount of entropy well after the inflaton reheating. In that case, the  $X$ -era is a short radiation-dominated era standing just after inflaton reheating and before the  $\sigma$  domination. For such a scenario, one has  $R_x = 1$  whereas, the  $Y$ -era would precisely correspond to the field domination era having  $w_y = 0$  such that  $R_y$  can only take negative values (quadratic potential). In Fig. 2 to Fig. 4 we have represented the WMAP7 constraints on the combination  $R_{\text{rad}}R_xR_y$  (for  $R_x = 1$ ) for various large field models, either massive as the scenario we are interested in, or for any values of  $p$ , the power law exponent of the inflaton potential. The method we have used is the same as in Ref. [3] and we do not repeat the details here. As already shown in Fig. 1, large values of  $|\Delta N_*|$ , which corresponds to  $R_{\text{rad}}R_y < 0$ , give bigger  $r$  and more red-tilted spectral index  $n_s$ . Hence smaller values of  $R_{\text{rad}}R_y$  are disfavored, which means that the current observations already give some constraints on the thermal history of the Universe. The posteriors for  $\rho_{\text{end}}$  are also depicted and since it is essentially determined by the amplitude of the curvature perturbation, it is well bounded [3].

In some literature, when one considers a late-time entropy production scenario, the parameter  $F$  is adopted to quantify the amount of entropy production, instead of  $R_y$ , and is defined as

$$F \equiv \frac{s_{\text{yend}} a_{\text{yend}}^3}{s_{\text{yini}} a_{\text{yini}}^3}. \quad (22)$$

The subscript “yini” and “yend” indicate that the quantities are the ones evaluated at the time when  $Y$ -era starts and ends. Contrary to the definition of the  $R_{\text{rad}}$  and  $R_x$  parameters which only require that total energy density is conserved, the definition of  $F$  is convenient if thermalization is achieved. In our scenario, at the beginning of the  $Y$ -era, and also just after its end, the Universe is assumed to be radiation dominated, and if thermalized, the entropy density is dominated by relativistic species. In that situation, it is straightforward to show that

$$R_y = F^{-1/3} \left( \frac{\mathcal{Q}_{\text{yini}}}{\mathcal{Q}_{\text{yend}}} \right)^{1/4}, \quad (23)$$

where  $\mathcal{Q}$  is defined as in Eq. (16) for the epochs of interest.

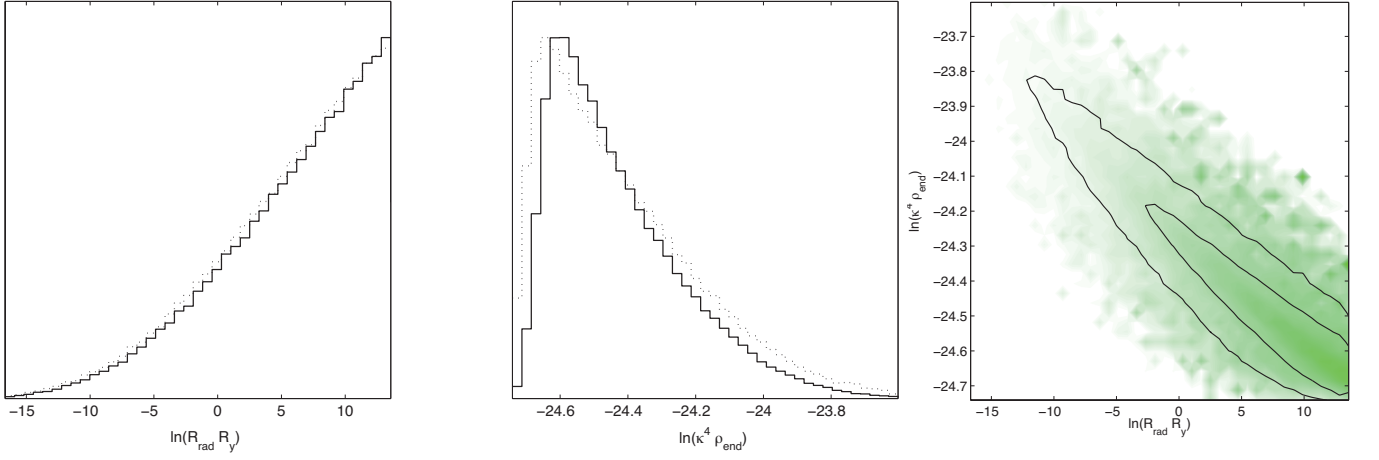


FIG. 2: Marginalized posterior probability distributions (solid line) and mean likelihood (dotted line) from WMAP7 and HST data for massive inflation with  $p = 2$ . The right figure shows the one- and two-sigma confidence intervals of the two-dimensional marginalized posterior in the plane  $(R_{\text{rad}} R_y, \kappa^4 \rho_{\text{end}})$ .

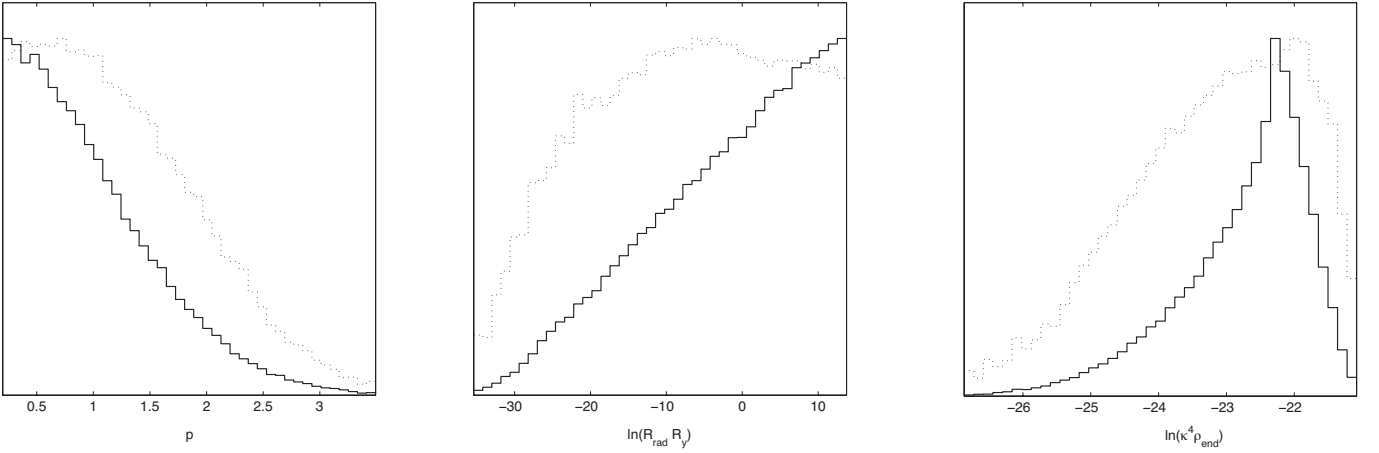


FIG. 3: Marginalized posterior probability distributions (solid line) and mean likelihood (dotted line) from WMAP7 and HST data for the large field potential with a power law exponent  $p$  being varied in  $0.2 < p < 5$ .

### B. Stochastic gravitational waves background

As discussed in the previous section, CMB can constrain the amount of entropy production but this will remain completely degenerated with reheating from the inflaton as the only quantities appearing in the determination of  $\Delta N_*$  is the product of  $R$  parameters such as  $R_{\text{rad}} R_x R_y$ . As we show below, this is not the same for stochastic gravitational waves of inflationary origin: they feel these parameters in a different way which can be used to break the degeneracies, thereby performing the tomography of the history of the Universe. In particular, direct detection experiments as BBO and DECIGO, which probe the frequency range  $f \sim \mathcal{O}(1)$  Hz, would give new and complementary information with respect to CMB.

In order to discuss the amplitude of stochastic GW, one

usually uses the spectrum of the energy density of GW normalized by the critical energy density  $\rho_{\text{crit}}$ . From the pseudo stress-tensor, assuming a stochastic background in which spatial and time averages are identical, one gets [25, 26]

$$\begin{aligned} \Omega_{\text{gw}} &\equiv \frac{1}{\rho_{\text{crit}}} \frac{d\rho_{\text{gw}}}{d \ln k} = \frac{1}{12} \left( \frac{k}{aH} \right)^2 \frac{k^3}{\pi^2} \sum_{\lambda} |h_{\lambda}|^2 \\ &= \frac{1}{12} \left( \frac{k}{aH} \right)^2 \mathcal{P}_h^{(\text{obs})}(k). \end{aligned} \quad (24)$$

The observed power spectrum  $\mathcal{P}_h^{(\text{obs})}$  at the time of interest (e.g. today) is given by Eq. (5) times a transfer function encoding the evolution of the sub-Hubble modes

$$\mathcal{P}_h^{(\text{obs})}(k) = \mathcal{P}_h(k) \mathcal{T}^2(k). \quad (25)$$

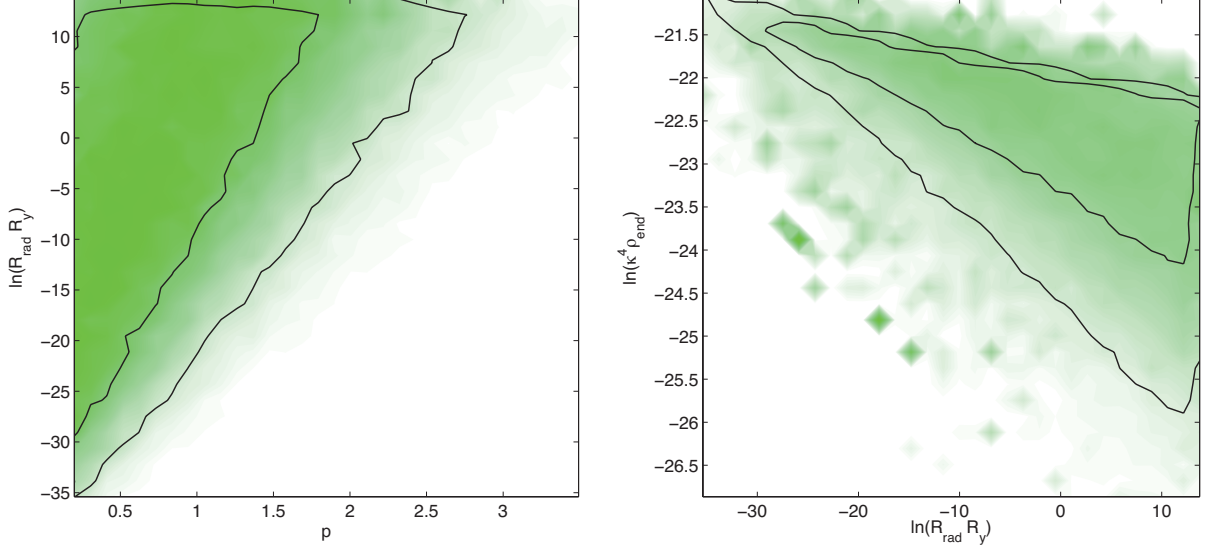


FIG. 4: Two-dimensional posteriors with  $1\sigma$  and  $2\sigma$  confidence regions from WMAP7 and HST data in the  $(p, R_{\text{rad}} R_y)$  plane (left) and in the  $(R_{\text{rad}} R_y, \kappa^4 \rho_{\text{end}})$  plane (right).

The transfer function  $\mathcal{T}$  can be evaluated analytically since, after inflation, the tensor perturbations are decoupled from other sources and their equation of evolution in Fourier space is given by

$$h'' + 2\mathcal{H}h' + k^2 h = 0, \quad (26)$$

where for simplicity the polarization index has been dropped. Assuming for the moment that the background is dominated by a fluid having a constant equation of state parameter  $w$ , the solution reads

$$h(\eta, \mathbf{k}) \propto (k\eta)^{(3w-3)/(6w+2)} J_{\frac{3-3w}{6w+2}}(k\eta). \quad (27)$$

For super-Hubble modes ( $k\eta \ll 1$ ) we recover that  $h(\eta, \mathbf{k})$  is constant while for sub-Hubble wavenumbers one has

$$|h(\eta, \mathbf{k})|^2 \underset{k\eta \gg 1}{\propto} a^{-2}. \quad (28)$$

Since  $h$  stays constant on super-Hubble scales, the transfer function is determined only by the era at which a given mode  $k$  reenters the Hubble radius. Every mode  $k$  will then be damped till the present time by a factor  $(a_k/a_0)^2$  where  $a_k$  is solution of

$$k = a_k H(a_k), \quad (29)$$

and the scale factor today will be taken as unity  $a_0 = 1$ .

#### 1. Radiation and matter eras

We start with the case for which the mode reenters during radiation era. Assuming an instantaneous

transition, the result can be approximated by squaring Eq. (29) and using the first Friedmann–Lemaître equation,  $H^2 = \rho/(3M_{\text{pl}}^2)$ . One gets

$$a_k^2 = \frac{3M_{\text{pl}}^2 k^2}{\rho(a_k)} = \frac{3M_{\text{pl}}^2 k^2}{\rho_{\text{eq}} a_{\text{eq}}^4} a_k^4, \quad (30)$$

where  $\rho \propto a^{-4}$  is used. The solution reads

$$a_k = a_{\text{eq}} \frac{k_{\text{eq}}}{k} = \frac{1}{1+z_{\text{eq}}} \frac{k_{\text{eq}}}{k}, \quad (31)$$

with

$$k_{\text{eq}} \equiv \frac{1}{\sqrt{3}M_{\text{pl}}} \frac{\sqrt{\rho_{\text{eq}}}}{1+z_{\text{eq}}} \simeq H_0 \frac{\Omega_{\text{m}0}}{\sqrt{\Omega_{\text{r}0}}}. \quad (32)$$

In the rightmost side,  $\Omega_{\text{m}0}$  and  $\Omega_{\text{r}0}$  are the matter and radiation density parameters today and  $\rho_{\text{eq}} \simeq 2\rho_{\gamma 0}/a_{\text{eq}}^4$  is the energy density at equality. For all modes entering the Hubble radius in the radiation era, Eq. (31) immediately gives the transfer function for  $k > k_{\text{eq}}$  [27]:

$$\mathcal{T}_{\text{rad}}(k) \simeq H_0^2 \Omega_{\text{m}0} \frac{k_{\text{eq}}}{k} \simeq \frac{H_0 \sqrt{\Omega_{\text{r}0}}}{k}, \quad (33)$$

Similarly, starting from Eq. (29), the matter era solution reads

$$\mathcal{T}_{\text{mat}}(k) \simeq \frac{H_0^2 \Omega_{\text{m}0}}{k^2} \Theta(k < k_{\text{eq}}), \quad (34)$$

where  $\Theta(x)$  is the Heaviside step function. In fact, considering a mixture of radiation and matter, one would

find

$$\mathcal{T}_{\text{eq}}(k) \simeq \frac{H_0^2 \Omega_{\text{m}0}}{2k^2} \left[ 1 + \sqrt{1 + 4 \left( \frac{k}{k_{\text{eq}}} \right)^2} \right], \quad (35)$$

which gives back Eqs. (33) and (34) in the appropriate limits. Although not specified, the above transfer functions are unity for super-Hubble modes, i.e.  $k < H_0^{-1}$ . Combined with Eq. (24) we recover the well-known result [26] that  $\Omega_{\text{gw}}$  is constant for  $k > k_{\text{eq}}$  and decays as  $k^{-2} \propto f^{-2}$  for modes entering during matter domination.

The same line of reasoning can be applied to the post-inflationary universe assuming the non-standard history. Just after reheating we assume the universe to be in a  $X$ -era (radiation-dominated in our scenario), then becomes  $Y$ -dominated, e.g. driven by an oscillating scalar field, which finally decays into radiation.

## 2. Non-standard post-inflationary eras

If an observable mode today entered the Hubble radius during the  $Y$ -era, Eq. (29) can be dealt exactly as the radiation-era case, provided  $w_Y$  remains constant. The equivalent of Eq. (30) now reads

$$a_k^2 = \frac{3M_{\text{pl}}^2 k^2}{\rho_{\text{yend}} a_{\text{yend}}^{3+3w_Y}} a_k^{3+3w_Y}, \quad (36)$$

whose solution can be recast into

$$a_k = a_{\text{yend}} \left( \frac{k_{\text{yend}}}{k} \right)^{2/(1+3w_Y)}. \quad (37)$$

This expression can be further simplified by remarking that

$$a_{\text{yend}} = a_0 \mathcal{Q}_{\text{yend}}^{1/4} \left( \frac{\rho_{\gamma_0}}{\rho_{\text{yend}}} \right)^{1/4}, \quad (38)$$

since the end of the  $Y$ -era matches with the beginning of the standard radiation dominated era. The wavenumber  $k_{\text{yend}}$  correspond to a mode entering the Hubble radius just at the end of the  $Y$ -era, i.e. at the beginning of the radiation era:

$$k_{\text{yend}} \equiv \frac{a_{\text{yend}}}{\sqrt{3}M_{\text{pl}}} \sqrt{\rho_{\text{yend}}} = \frac{1}{\sqrt{3}M_{\text{pl}}} (\tilde{\rho}_{\gamma_0} \rho_{\text{yend}})^{1/4}, \quad (39)$$

where the last equality comes from Eq. (38). At this point, Eq. (37) shows that the quantities  $k_{\text{yend}}$  and  $w_Y$  are observable and completely determined by the measurement of  $\Omega_{\text{gw}}(k)$ . As a result, we should try to express all quantities in terms of them, and in particular the redshift at which the  $Y$ -era ended. From Eq. (38), one gets

$$1 + z_{\text{yend}} = \sqrt{3} \frac{k_{\text{yend}} M_{\text{pl}}}{\tilde{\rho}_{\gamma_0}^{1/2}}. \quad (40)$$

We finally get the transfer function during the  $Y$ -era

$$\mathcal{T}_Y(k) \simeq \frac{\tilde{\rho}_{\gamma_0}^{1/2}}{\sqrt{3} k_{\text{yend}} M_{\text{pl}}} \left( \frac{k_{\text{yend}}}{k} \right)^{2/(1+3w_Y)} \Theta(k > k_{\text{yend}}) + \Theta(k < k_{\text{yend}}). \quad (41)$$

It remains now to deal with the modes entering the Hubble radius before, i.e. either during  $X$  domination or during reheating. The calculations are again the same although the scale factor at the end of the  $X$ -era reads

$$a_{\text{xend}} = a_{\text{yend}} \frac{a_{\text{xend}}}{a_{\text{yend}}} = a_{\text{yend}} R_Y \left( \frac{\rho_{\text{yend}}}{\rho_{\text{yini}}} \right)^{1/4}, \quad (42)$$

where Eq. (21) has been used for  $a_{\text{xend}}/a_{\text{yend}}$ . One can further simplify this expression by using Eq. (38) to get

$$a_{\text{xend}} = R_Y \left( \frac{\tilde{\rho}_{\gamma_0}}{\rho_{\text{xend}}} \right)^{1/4}. \quad (43)$$

Defining  $k_{\text{xend}}$  the wavenumber of a mode entering the Hubble radius at the end of the  $X$ -era, we have

$$k_{\text{xend}} \equiv \frac{a_{\text{xend}}}{\sqrt{3}M_{\text{pl}}} \sqrt{\rho_{\text{xend}}} = \frac{R_Y}{\sqrt{3}M_{\text{pl}}} (\tilde{\rho}_{\gamma_0} \rho_{\text{xend}})^{1/4}, \quad (44)$$

such that the corresponding redshift can be expressed in terms of observable quantities as

$$1 + z_{\text{xend}} = \sqrt{3} \frac{k_{\text{xend}} M_{\text{pl}}}{R_Y^2 \tilde{\rho}_{\gamma_0}^{1/2}}. \quad (45)$$

The transfer function during this era is again given by  $|a_k|$  and reads

$$\mathcal{T}_X(k) \simeq \frac{R_Y^2 \tilde{\rho}_{\gamma_0}^{1/2}}{\sqrt{3} k_{\text{xend}} M_{\text{pl}}} \left( \frac{k_{\text{xend}}}{k} \right)^{2/(1+3w_X)} \Theta(k > k_{\text{xend}}) + \Theta(k < k_{\text{xend}}). \quad (46)$$

Finally, in order to deal with modes entering the Hubble radius during reheating (inflaton oscillation dominated era), we similarly express  $a_{\text{reh}}$  in terms of  $a_{\text{xend}}$  to get

$$a_{\text{reh}} = R_X R_Y \left( \frac{\tilde{\rho}_{\gamma_0}}{\rho_{\text{reh}}} \right)^{1/4}. \quad (47)$$

Again, the wavenumber crossing the end of reheating is given by

$$k_{\text{reh}} \equiv \frac{a_{\text{reh}}}{\sqrt{3}M_{\text{pl}}} \sqrt{\rho_{\text{reh}}} = \frac{R_X R_Y}{\sqrt{3}M_{\text{pl}}} (\tilde{\rho}_{\gamma_0} \rho_{\text{reh}})^{1/4}, \quad (48)$$

and the redshift at which reheating ended reads

$$1 + z_{\text{reh}} = \sqrt{3} \frac{k_{\text{reh}} M_{\text{pl}}}{R_X^2 R_Y^2 \tilde{\rho}_{\gamma_0}^{1/2}}. \quad (49)$$

Therefore, the transfer function during reheating is

$$\mathcal{T}_{\text{reh}}(k) \simeq \frac{R_x^2 R_y^2 \rho_{\gamma 0}^{-1/2}}{\sqrt{3} k_{\text{reh}} M_{\text{pl}}} \left( \frac{k_{\text{reh}}}{k} \right)^{2/(1+3w_{\text{reh}})} \Theta(k > k_{\text{reh}}) + \Theta(k < k_{\text{reh}}), \quad (50)$$

which shows the influence of  $R_x$  and  $R_y$ , making them observable in the gravitational wave spectrum. However, contrary to CMB, they are no longer degenerated with  $R_{\text{rad}}$ . Conversely, using both CMB and  $\Omega_{\text{gw}}$ , one expects to be able to disambiguate the effects of  $R_{\text{rad}}$ ,  $R_x$  and  $R_y$ . The same reasoning could be extended to another  $Z$ -era inserted somewhere.

To summarize, one finally gets

$$\Omega_{\text{gw}}(k) \simeq \frac{k^2}{12H_0^2} \mathcal{T}_{\text{eq}}^2(k) \mathcal{T}_y^2(k) \mathcal{T}_x^2(k) \mathcal{T}_{\text{reh}}^2(k) \mathcal{P}_h(k), \quad (51)$$

where the three transfer functions are given by Eqs. (35), (41), (46) and (50) and their respective pivot wavenumbers by Eqs. (32), (39), (44) and (48). All of those four wavenumbers therefore correspond to frequencies of the gravitational wave  $f_{\text{eq}}$ ,  $f_{\text{yend}}$ ,  $f_{\text{xend}}$  and  $f_{\text{reh}}$ .

### III. FORECASTS ON THERMAL HISTORY FROM FUTURE CMB AND GW EXPERIMENTS

In this section, we discuss how and to what extent we can probe the thermal history of the Universe with future CMB and direct detection of GW experiments.

#### A. An illustrative scenario

For illustrative purposes, we consider in the following the specific scenario mentioned earlier. Inflation is driven by a massive field  $\phi$  having the potential  $V(\phi) = (1/2)m^2\phi^2$  with  $m$  being the inflaton mass. Furthermore there also exists another scalar field, denoted as  $\sigma$  that comes to dominate the universe at later times. After inflation,  $\phi$  oscillates around the minimum of its potential and the reheating (inflaton oscillation dominated) era is matter-like [28] till the Universe thermalizes and becomes radiation-dominated (the  $X$ -era). The reheating temperature  $T_{\text{reh}}$ , associated with the energy density  $\rho_{\text{reh}}$ , refers to the time at which the reheating era ends and the radiation  $X$ -era starts. Then the field  $\sigma$  begins to oscillate at some epoch and starts the  $\sigma$  oscillation dominated era, referred to as the  $Y$ -era in the previous section. We moreover assume that  $\sigma$  decays after it dominates the Universe to start the usual radiation dominated period. Thus, the thermal history of the Universe proceeds as follows: Inflation  $\rightarrow$  reheating era (oscillating  $\phi$  dominated era)  $\rightarrow$  RD ( $X$ -era)  $\rightarrow$  Oscillating  $\sigma$  dominated era ( $Y$ -era)  $\rightarrow$  RD era. The final RD era continues until the radiation-matter equality, just before the recombination epoch. As discussed in the previous section, depending

on the duration of each era, the predictions for CMB and GW spectra are different, from which we can probe the thermal history.

Under these hypothesis, we can express all the quantities of the previous section in terms of temperatures and frequencies. With  $R_x = 1$ , assuming that  $g = g_s = g_*$  at the time of “yend,” “xend,” and “reh” and using Eq. (22), Eqs. (39), (44) and (48), one obtains

$$\begin{aligned} f_{\text{yend}} &\simeq 0.2 \text{ Hz} \left( \frac{g_{*\text{yend}}}{100} \right) \left( \frac{T_\sigma}{10^7 \text{ GeV}} \right), \\ f_{\text{xend}} &\simeq 0.2 \text{ Hz} \left( \frac{g_{*\text{yend}}}{100} \right) \left( \frac{T_\sigma}{10^7 \text{ GeV}} \right) F^{2/3}, \\ f_{\text{reh}} &\simeq 0.2 \text{ Hz} \left( \frac{g_{*\text{yend}}}{100} \right) \left( \frac{T_{\text{reh}}}{10^7 \text{ GeV}} \right) F^{-1/3}, \end{aligned} \quad (52)$$

where  $T_\sigma$  is the temperature at which  $\sigma$  decays into radiation.

For CMB constraints, one can also simplify the quantity  $R_{\text{rad}} R_y$  in terms of temperatures as

$$\begin{aligned} \ln(R_{\text{rad}} R_y) &= \frac{1}{3} \ln \frac{T_{\text{reh}}}{M_{\text{pl}}} - \frac{1}{3} \ln F \\ &\quad - \frac{1}{12} \ln \frac{\rho_{\text{end}}}{M_{\text{pl}}^4} + \frac{1}{12} \ln \left( \frac{\pi^2}{30} \frac{g_{*\text{reh}} g_{*\text{yend}}}{g_{*\text{xend}}} \right), \end{aligned} \quad (53)$$

where  $\bar{w}_{\text{reh}} = 0$  has been used. Since  $T_{\text{reh}}$  is assumed to be bigger than  $T_\sigma$ , we have the expected hierarchy  $f_{\text{reh}} > f_{\text{xend}} > f_{\text{yend}}$ . For the effective degrees of freedom, we assume those of the standard model of particle physics, i.e.,  $g_{*\text{reh}} = g_{*\text{xend}} = g_{*\text{yend}} = 106.75$  in the following analysis. Notice that this is certainly not verified but the influence of  $g_*$  remains very small in the final forecasts, the sensible quantities being logarithmic, see Eq. (53).

Some example plots for GW spectrum are shown in Fig. 5. The GW spectrum is obtained by numerically integrating Eq. (26), using the WKB approximation ( $h \propto e^{\pm i k \eta} / a$ ) for the oscillating phase. To see how the spectrum shape depends on the reheating temperatures and  $F$ , we show several cases for these parameters. For reference, the sensitivity frequency bands for BBO/FP-DECIGO and Ultimate DECIGO are also depicted (for the specifications of these experiments, see Table II). In some cases, the change of the spectrum can be traced with future experiments, in particular, for Ultimate DECIGO. In such a case, the parameters such as the reheating temperatures and  $F$  can be well determined, which is going to be studied by using Fisher matrix analysis in the following.

#### B. Fisher matrix analysis

To forecast constraints from future experiments, we use a Fisher matrix analysis for both CMB [29] and GW direct detection [30]. Under the assumption of a Gaussian likelihood, the Fisher matrix is given by the second



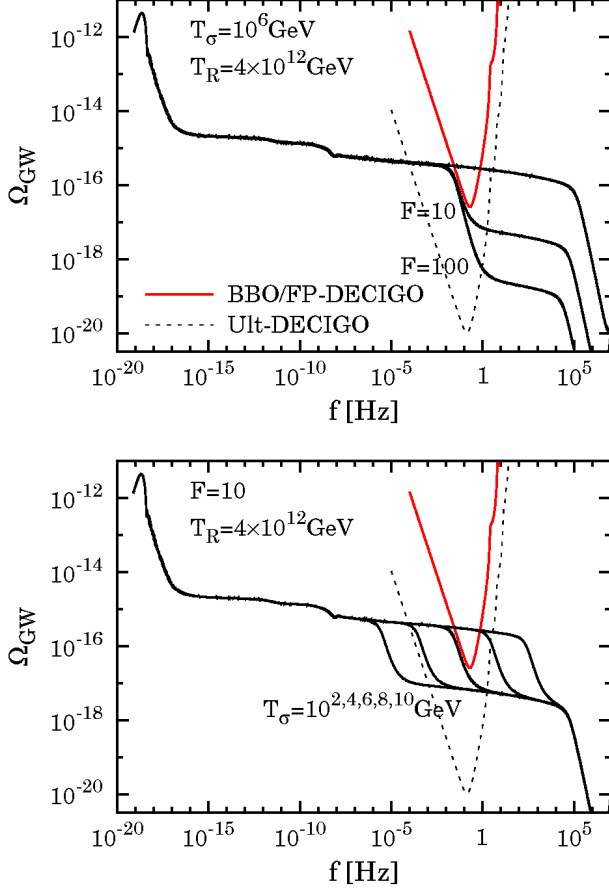


FIG. 5: GW spectrum for several values of  $F$  ranging from  $F = 0$  to  $F = 100$  at fixed  $T_\sigma$  (top). The bottom panel shows the spectra at fixed  $F = 10$  and for various values of  $T_\sigma$ . The reheating temperature  $T_{\text{reh}}$  from the inflaton is fixed at  $T_{\text{reh}} = 10^{12}$  GeV in these figures.

derivative of the log-likelihood with respect to the parameters  $p_i$  at the likelihood maximum,

$$\mathcal{F}_{ij} = - \left\langle \frac{\partial^2 \ln \mathcal{L}}{\partial p_i \partial p_j} \right\rangle, \quad (54)$$

and its inverse gives marginalized  $1\sigma$  error of the parameter of interest,

$$\sigma(p_i) = \sqrt{(\mathcal{F}^{-1})_{ii}}. \quad (55)$$

### 1. CMB experiment

In the case of CMB experiment, we assume that the Fisher matrix for both CMBpol and PLANCK is given by

$$\mathcal{F}_{ij} = \sum_{\ell=2}^{\ell_{\text{max}}} \sum_{XX', YY'} \frac{\partial C_\ell^{XX'}}{\partial p_i} (\text{Cov}_\ell^{-1})_{XX'YY'} \frac{\partial C_\ell^{YY'}}{\partial p_j}, \quad (56)$$

where  $X$  and  $X'$  are summed over the CMB temperature,  $E$ -mode polarization, and  $B$ -mode polarization ( $X = T, E, B$ ). The covariance matrix is given by

$$\begin{aligned} (\text{Cov}^{-1})_{TTTT} &= \frac{2}{(2l+1)f_{\text{sky}}} (C_\ell^{TT} + w_T^{-1} B_\ell^{-2})^2, \\ (\text{Cov}^{-1})_{EEEE} &= \frac{2}{(2l+1)f_{\text{sky}}} (C_\ell^{EE} + w_P^{-1} B_\ell^{-2})^2, \\ (\text{Cov}^{-1})_{BBBB} &= \frac{2}{(2l+1)f_{\text{sky}}} (C_\ell^{BB} + w_P^{-1} B_\ell^{-2})^2, \\ (\text{Cov}^{-1})_{TETE} &= \frac{2}{(2l+1)f_{\text{sky}}} [(C_\ell^{TE})^2 \\ &\quad + (C_\ell^{TT} + w_T^{-1} B_\ell^{-2})(C_\ell^{EE} + w_P^{-1} B_\ell^{-2})], \\ (\text{Cov}^{-1})_{TTEE} &= \frac{2}{(2l+1)f_{\text{sky}}} (C_\ell^{TE})^2, \\ (\text{Cov}^{-1})_{TTTE} &= \frac{2}{(2l+1)f_{\text{sky}}} C_\ell^{TE} (C_\ell^{TT} + w_T^{-1} B_\ell^{-2}), \\ (\text{Cov}^{-1})_{EETE} &= \frac{2}{(2l+1)f_{\text{sky}}} C_\ell^{TE} (C_\ell^{EE} + w_P^{-1} B_\ell^{-2}), \end{aligned} \quad (57)$$

where  $w_{(T,P)}^{-1} = 4\pi\sigma_{(T,P)}^2/N_{\text{pix}}$  is the variance of the noise temperature per pixel (in  $\mu\text{K}^2$ ). For simplicity, we have assumed a Gaussian beam  $B_\ell \simeq \exp[-\ell(\ell+1)\sigma_b^2/2]$  with  $\sigma_b = \theta/\sqrt{8\ln 2}$  being the beam width. In Table I, we list the values of the observed fraction of the sky  $f_{\text{sky}}$ , the temperature noise per pixel  $\sigma_T$ , the polarization noise per pixel  $\sigma_P$  and the Gaussian beam width  $\theta^2 = 4\pi/N_{\text{pix}}$  for Planck [31] and CMBpol [32] experiments that are adopted to derive our forecasts. The different frequency channels are combined according to  $w_{(T,P)} B_\ell^2 = \sum_\nu w_{(T,P)}^\nu (B_\ell^\nu)^2$ , where  $\nu$  refers to each channel component [33]. Finally, the maximum multipole value has been set to  $\ell_{\text{max}} = 2000$ .

Hereafter, we assume a flat  $\Lambda\text{CDM}$  Universe and set the fiducial cosmological parameters to the WMAP7 mean values [9].

### 2. GW direct detection

For the GW direct detection experiments, we will be considering three future experiments, FP-DECIGO, BBO and Ultimate-DECIGO [10–12]. FP-DECIGO is planned to be a Fabry-Perot Michelson interferometer, while BBO experiment will use time-delay interferometry (TDI). Although they use different technology, in this paper, we do not distinguish these experiments, since they have similar sensitivity. The Fisher matrix for GW direct detection is given by [30]

$$\begin{aligned} \mathcal{F}_{ij} &= \left( \frac{3H_0^2}{10\pi^2} \right)^2 2t_{\text{obs}} \\ &\quad \times \sum_{(I,J)} \int_0^\infty df \frac{|\gamma_{IJ}(f)|^2 \partial_{p_i} \Omega_{\text{gw}}(f) \partial_{p_j} \Omega_{\text{gw}}(f)}{f^6 S_I(f) S_J(f)}, \end{aligned} \quad (58)$$

TABLE I: Instrument parameter values for CMB experiments

Experiment	$f_{\text{sky}}$	Center frequency [GHz]	$\theta$ [FWHM arcmin]	$\sigma_T$ [ $\mu\text{K}$ ]	$\sigma_P$ [ $\mu\text{K}$ ]
Planck [31]	0.65	70	14	12.8	18.2
		100	10	6.8	10.9
		143	7.1	6.0	11.4
		217	5.0	13.1	26.7
CMBpol [32]	0.65	100	4.2	0.87	1.18
		150	2.8	1.26	1.76
		220	1.9	1.84	2.60

where  $\Omega_{\text{gw}}$  is given in Eq. (24) and  $t_{\text{obs}}$  is the observation time. The subscripts  $I$  and  $J$  refer to independent signals obtained at each detector, or observables generated by combining the detector signals. For a BBO-like experiment, the summation runs over the TDI channel output index ( $I = A, E, T$ ) [30]. The overlap reduction  $\gamma_{IJ}(f)$  for TDI variables is calculated following the procedure of Ref. [34]. For the cross term ( $I \neq J$ ), we have  $\gamma_{IJ}(f) = 0$ . The noise spectrum  $S_{I,J}(f)$  is given by

$$\begin{aligned}
S_A(f) &= S_E(f) = 8 \sin^2(\hat{f}/2) \left\{ (2 + \cos \hat{f}) S_{\text{shot}} \right. \\
&\quad \left. + 2 \left[ 3 + 2 \cos \hat{f} + \cos(2\hat{f}) \right] S_{\text{accel}} \right\}, \\
S_T(f) &= 2 \left( 1 + 2 \cos \hat{f} \right)^2 \left[ S_{\text{shot}} + 4 \sin^2(\hat{f}/2) S_{\text{accel}} \right],
\end{aligned} \tag{59}$$

where  $\hat{f} = 2\pi L f$ . The values of the arm length  $L$ , the shot noise  $S_{\text{shot}}$  and the radiation pressure noise  $S_{\text{accel}}$  have been reported in Table II for BBO/FP-DECIGO and Ultimate-DECIGO, respectively. One may be concerned about the noise contamination from white dwarf binaries at frequencies below  $\sim 0.1$  Hz, and introduce a low-frequency cutoff to the integral. However, it may be possible to remove it by identifying all binaries and subtracting their contributions from data streams [35–37]. In this paper, we assume that this is the case and do not introduce such a low-frequency cutoff.

Although we focus on the inflationary GW background in this paper, it should also be noted that there may be other possible GW signals in the sensitivity range of BBO and DECIGO. Such examples include for instance first order phase transition [38–42], preheating [43–47], particle production [48] and cosmic strings [49–53]. These GWs may be significant in some cases but they will not be considered in the following.

### C. Forecasts on early Universe history

Now we investigate the constraint on the thermal history of the Universe using the Fisher matrix method discussed in the previous section. For this purpose, we focus on the reheating temperature  $T_{\text{reh}}$  associated with the inflaton, the temperature associated with the second field

$T_\sigma$ , and the amount of late-time entropy production  $F$  (or equivalently  $R_\gamma$ ).

#### 1. Unobservable spectral features

In this section, we have performed a Fisher analysis to obtain the expected constraints from Planck/CMBpol for CMB and BBO/DECIGO for GW direct detection. As a fiducial model for the analysis, we consider two cases with  $g_{* \text{reh}}^{1/4} T_{\text{reh}} \sim 10^{16}$  GeV (corresponding to  $N \equiv -\Delta N_* \sim 57$ ) and  $g_{* \text{reh}}^{1/4} T_{\text{reh}} \sim 10^9$  GeV (corresponding to  $N \sim 52$ ), assuming that there is no late-time entropy production, i.e.,  $F = 1$ .

For the above fiducial models, there is no spectral signatures in the sensitivity range of the GWs direct detection experiments and the Fisher analysis remain insensitive to any information coming from the spectral shapes. As a result, one expects some degeneracies to occur between the model parameters. In Figs. 6 and 7, we have represented the  $2\sigma$  allowed regions in the plane  $(T_{\text{reh}}, F)$  and  $(m, F)$ , respectively, for several combinations of those future data.

There are two cases to consider according to the values of  $T_\sigma$ . In Fig. 6, we have also represented the region where the signal-to-noise ratio is  $S/N > 5$  for BBO/FP-DECIGO as the light blue shaded region. As studied in Fig. 5, a late time entropy production would induce a suppression of the GW spectrum amplitude at frequencies higher than  $f_{\text{yend}}$ , which corresponds to  $T_\sigma$  in Eq. (52). For BBO/FP-DECIGO, the suppression occurs in the sensitivity region when  $T_\sigma < 10^6$  GeV. In that situation, a direct detection of the primordial GWs by BBO/FP-DECIGO would immediately yield a strong upper bound for  $F \lesssim 2.4$  (see Fig. 6). At the same time, since the reheating also induces a suppression of the GWs spectrum amplitude, direct detection would readily excludes  $T_{\text{reh}} < 10^6$  GeV for the same reason.

The opposite situation, i.e. the case with  $T_\sigma > 10^6$  GeV, the spectrum is suppressed at higher frequencies and beyond the sensitivity range of the experiment. Therefore, the amplitude of the observable GWs spectrum remains mostly independent of the values of  $F$ . In this case, direct detection of GWs still allows a large pa-

TABLE II: Instrument parameters for GW experiments

Experiments	$S_{\text{shot}} [(L/\text{km})^{-2}\text{Hz}^{-1}]$	$S_{\text{accel}} [(2\pi f/\text{Hz})^{-4}(2L/\text{km})^{-2}\text{Hz}^{-1}]$	$L [\text{km}]$
BBO/FP-DECIGO [34]	$2 \times 10^{-40}$	$9 \times 10^{-40}$	$5 \times 10^4$
Ultimate DECIGO [54]	$9 \times 10^{-44}$	$9 \times 10^{-44}$	$5 \times 10^4$

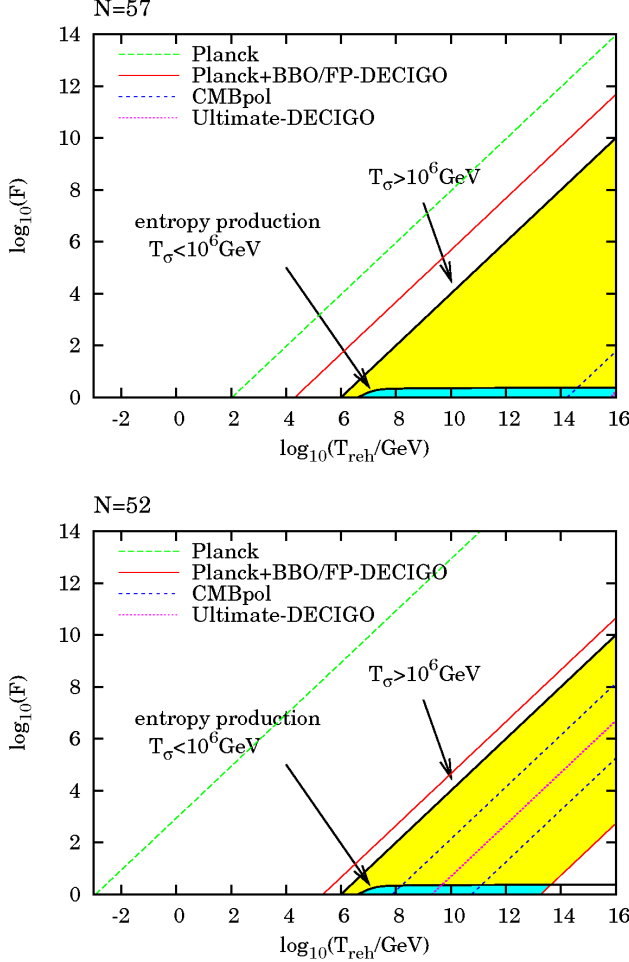


FIG. 6: Future constraints on the  $(T_{\text{reh}}, F)$  plane from CMB (Planck and CMBpol) and/or direct detection of GW (BBO/FP-DECIGO and Ultimate DECIGO). The light shaded region traces the  $2\sigma$  confidence interval of the two-dimensional marginalized posterior under the Fisher matrix analysis. For the darker blue shaded region traces the parameter space in which the signal-to-noise ratio  $S/N > 5$  (see text).

parameter space represented as the light yellow shading in Fig. 6. Within this region, the upper limit of  $F$ , equivalently the lower limit of  $T_{\text{reh}}$ , is imposed by the consideration that reheating should end before the late-time entropy production begins. In other words,  $f_{\text{xend}} < f_{\text{reh}}$  gives  $T_\sigma F^{2/3} < T_{\text{reh}} F^{-1/3}$  using Eq. (52), and given

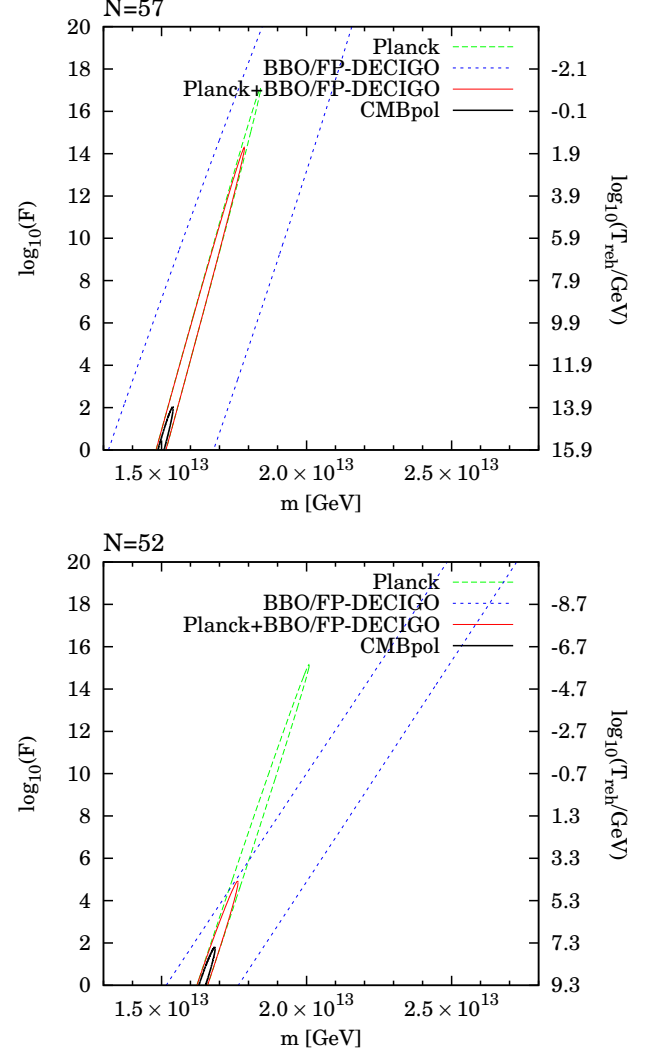


FIG. 7: Future constraint in the plane  $(m, F)$  from CMB (Planck and CMBpol) and GW (BBO/FP-DECIGO), for the two fiducial models having  $T_{\text{reh}} \simeq 10^9 \text{ GeV}$  ( $N = 52$ ) and  $T_{\text{reh}} \simeq 10^{16} \text{ GeV}$  ( $N = 57$ ).

$T_\sigma > 10^6 \text{ GeV}$ , we get  $T_{\text{reh}}/F > 10^6 \text{ GeV}$ . Since the constraints on  $F$  are completely degenerated with the one on  $T_{\text{reh}}$ , we have also reported the values of  $T_{\text{reh}}$  along the right vertical axis of Fig. 7.

Regarding CMB constraints, there is also a degeneracy between  $T_{\text{reh}}$  and  $F$ , which is clear from Eq. (53). However, the inflaton mass  $m$  can be probed through the amplitude of primordial curvature perturbation while  $n_s$

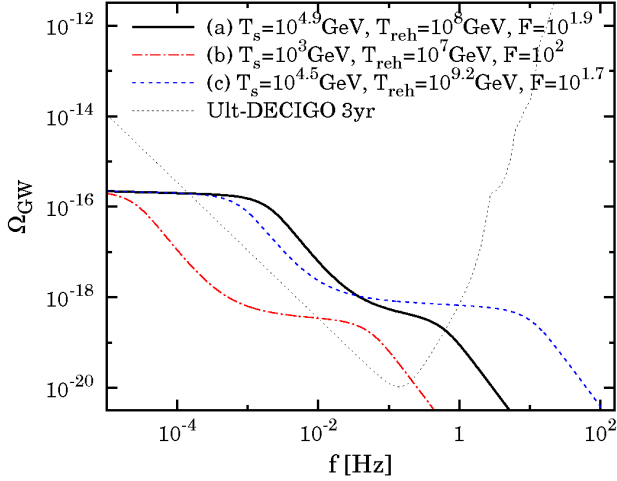


FIG. 8: Spectra of the three fiducial models (a), (b) and (c) together with the sensitivity region of the Ultimate-DECIGO GW experiment (see text). The corresponding forecasts are represented in Fig. 9.

and  $r$  are related to  $F$  and  $T_{\text{reh}}$ . On the other hand, the constraints from GW experiments basically come from their sensitivity to  $r$  and  $n_T$ . Since in the single field inflation model, these two quantities are related by  $n_T = -r/8$  (at leading order in slow-roll parameters),  $m$  and  $F$  are constrained in a different way compared to CMB. In addition, CMB and GW direct detection experiments measure slow-roll parameters quantities at different scales. As a result, the direction of this degeneracy differs thereby showing the complementarity of these observables.

## 2. Detection of spectral features

For Ultimate-DECIGO, the suppression region of the GW signal occurs at  $T_\sigma < 10^3$  GeV. However, there are large possibilities that the extreme sensitivity of Ultimate-DECIGO enables us to measure some of the spectral features. In that case, the detection of GWs would provide a precise determination of the parameters [55]. In the following, we investigate in more details the determination of the thermal history parameters by Ultimate-DECIGO in combination with CMBpol.

In Fig. 9, we show the constraints on the parameters  $T_{\text{reh}}$  and  $F$  expected from Ultimate-DECIGO together with ones expected from CMBpol. Three different fiducial models have been considered:

- (a) Both transition frequencies are inside the sensitivity frequency band of the experiment. We use the fiducial values  $T_\sigma = 10^{4.9}$  GeV,  $T_{\text{reh}} = 10^8$  GeV and  $F = 10^{1.9}$ .
- (b) The frequency  $f_{\text{xend}}$  is outside the sensitivity

range. As such an example, we consider the case with  $T_\sigma = 10^3$  GeV,  $T_{\text{reh}} = 10^7$  GeV and  $F = 10^2$ .

- (c) The frequency  $f_{\text{reh}}$  is outside the sensitivity range, which occurs for the fiducial values  $T_\sigma = 10^{4.5}$  GeV,  $T_{\text{reh}} = 10^{9.2}$  GeV and  $F = 10^{1.7}$ .

The spectra of these three models have been represented in Fig. 8. Here, we take  $T_{\text{reh}}$ ,  $F$ ,  $T_\sigma$  and  $m$  as free parameters and the predicted constraints are obtained by marginalizing over the remaining parameters. For CMBpol, the other cosmological parameters are also marginalized.

In the case (a), all features of the reheating and late-time entropy production are within the GW sensitivity range. Since, in this case, Ultimate-DECIGO alone can well determine all the parameters, we do not show the constraint from CMBpol alone (in fact, the  $1\sigma$  contour from CMBpol ends up being outside the range of the figure). However, it should be noted here that adding CMB data improves the constraint, as seen from the figure.

For the case (b), the damping of the GW spectrum within the sensitivity zone is due to the inflationary reheating and  $T_{\text{reh}}$  can be inferred. On the other hand, we find that GW measurements alone cannot determine the value of  $F$ , since the feature of late-time entropy production is now outside the region of detectability. However, if we combine CMB data, the constraint can be improved as seen from second panel of Fig. 9. To illustrate this more clearly, we show in Fig. 10 the marginalized constraints for case (b) in the  $(m, F)$  plane. Constraints from direct detection have a strong parameter degeneracy between  $m$  and  $F$ , since they both cause suppression of the amplitude of GWs at the maximum sensitivity region of Ultimate-DECIGO. However, CMB data such as CMBpol are strongly sensitive to the value of  $m$  and greatly helps to break the degeneracy. Therefore, although CMBpol data alone only provides constraints on  $F$  and  $T_{\text{reh}}$  with large uncertainties (see middle panel of Fig. 9), it can significantly tighten the constraints from Ultimate-DECIGO through improving the determination on  $m$ .

In the case (c), the reheating frequency is outside the sensitivity region such that the value of  $T_{\text{reh}}$  can no longer be well determined by GW measurements. Still  $T_\sigma$  and  $F$  can be well probed instead. As a result, the constraint from Ultimate DECIGO lies parallel to the  $T_{\text{reh}}$  axis (see Fig. 9). However, as repeatedly emphasized above, CMB probes the parameters differently from GW, thus in combination with CMBpol,  $T_{\text{reh}}$  can again be inferred and this ends up with breaking its degeneracy with  $F$ . Furthermore, in Fig. 11, we have also depicted the expected constraints in the  $(m, T_\sigma)$  plane, which also clearly illustrates the complementarity of observations of CMB and GW.

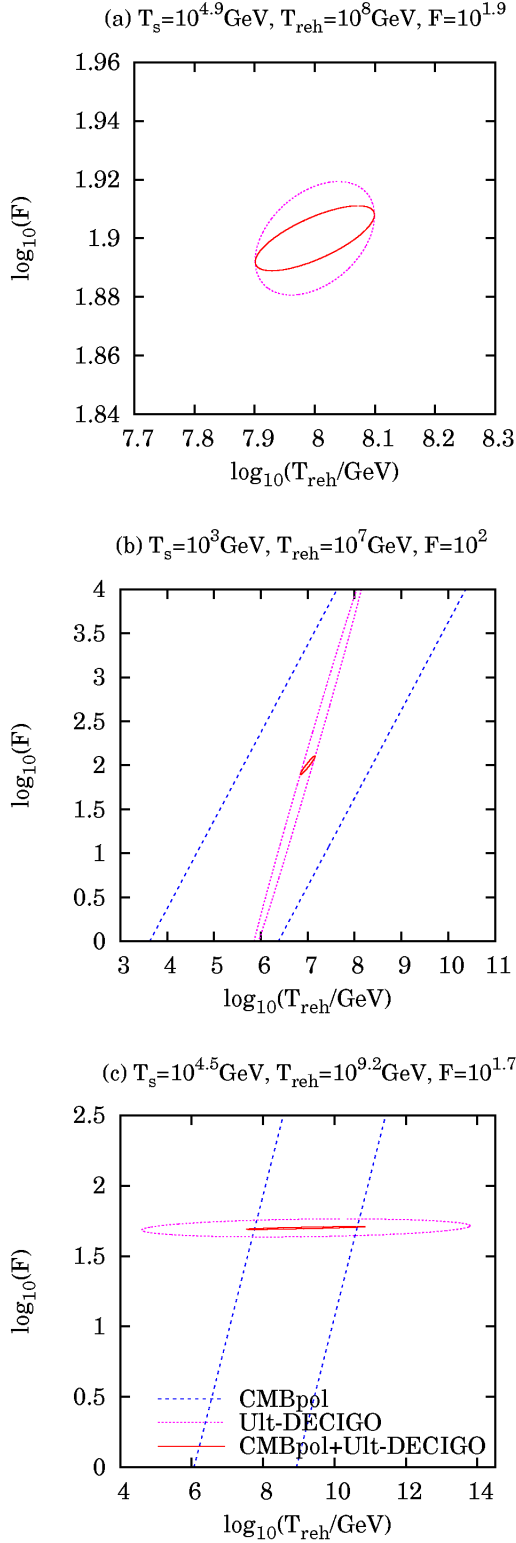


FIG. 9: Predicted constraints in the  $(T_{\text{reh}}, F)$  plane for the three different fiducial models (a), (b) and (c). The dotted and dashed lines show the marginalized  $2\sigma$  confidence contours expected from Ultimate-DECIGO and CMBpol, respectively. The solid line is the combined constraints. See also Fig. 10.

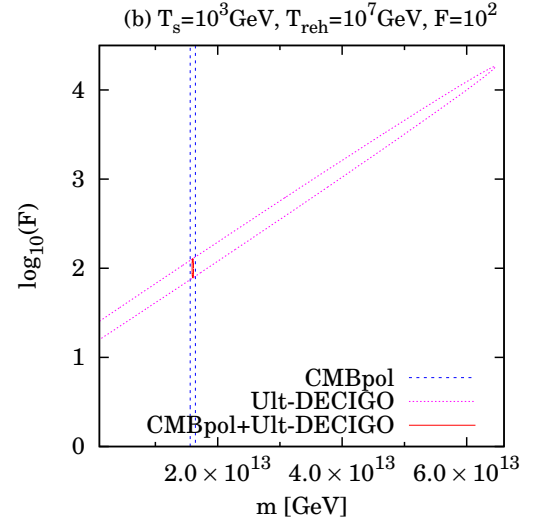


FIG. 10: Predicted constraints for the fiducial model (b) in the  $(m, F)$  plane for Ultimate-DECIGO, CMBpol and both (same convention as in Fig. 9).

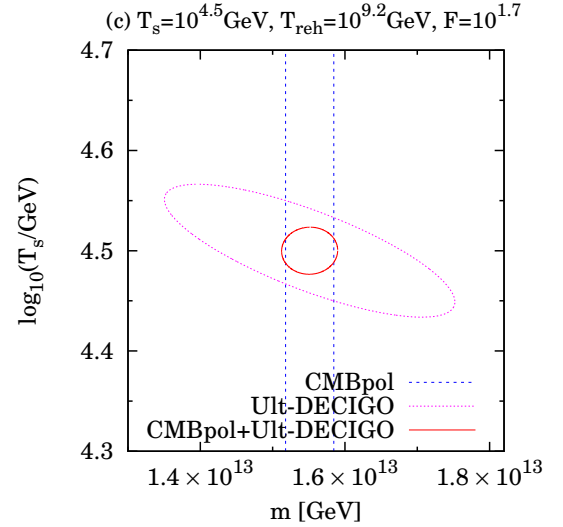


FIG. 11: Predicted constraints for the fiducial model (c) in the  $(m, T_s)$  plane for Ultimate-DECIGO, CMBpol and both (same convention as in Fig. 9).

#### IV. SUMMARY

We have discussed how one can probe the thermal history of the Universe from the era just after the end of inflation until the BBN epoch. In any given inflationary models, the spectral index and the tensor-to-scalar ratio are related to the  $e$ -fold number at which a reference scale exited the Hubble radius during inflation, thus in turn, they give a constraint on the total expansion of the scale factor since the above-mentioned epoch. By assuming chaotic inflation, we have presented how the

CMB is constraining the thermal history when there is an epoch of late-time entropy production, as for instance, a scenario where an oscillating scalar field dominates the Universe at some epoch, and then it decays.

In the future, direct detection GW experiments are expected to provide new cosmological probes, in addition to more precise CMB experiments such as Planck and CMBpol. Although CMB data can be used to determine the total amount of the cosmic expansion, they are only sensitive to the integrated thermal history and an epoch of late-time entropy production remains fully degenerated with the standard inflationary reheating era. This is not the case for GW experiments as they are precisely sensitive to the transition between these epochs. In particular, for the scenario with late-time entropy production, the GW spectrum bends twice at some transition frequencies (see Figs. 5 and 8). We have shown that if one, or more, frequencies do not lie in the GW experiment sensitivity region, CMB experiments can still greatly help to break the degeneracy. As shown in this paper, future

experiments of GW and CMB are complementary in performing a tomography of the thermal history between the end of inflation and BBN. As such, they are expected to play a major role in our understanding of the whole history of the Universe.

### Acknowledgments

T.T. would like to thank CP3 at Louvain University for the hospitality during the visit where a part of the work has been done. This work is partially supported by the Grant-in-Aid for Scientific research from the Ministry of Education, Science, Sports, and Culture, Japan, Nos. 23340058 (S.K.) and 24740149 (S.K.) and 23740195 (T.T). C.R. is partially supported by the ESA Belgian Federal PRODEX Grant No. 4000103071 and the Wallonia-Brussels Federation grant ARC No. 11/15-040.

- 
- [1] J. Martin and C. Ringeval, JCAP **0608**, 009 (2006), astro-ph/0605367.
  - [2] C. Ringeval, Lect. Notes Phys. **738**, 243 (2008), astro-ph/0703486.
  - [3] J. Martin and C. Ringeval, Phys. Rev. **D82**, 023511 (2010), 1004.5525.
  - [4] N. Seto and J. Yokoyama, J.Phys.Soc.Jap. **72**, 3082 (2003), gr-qc/0305096.
  - [5] K. Nakayama, S. Saito, Y. Suwa, and J. Yokoyama, Phys.Rev. **D77**, 124001 (2008), 0802.2452.
  - [6] K. Nakayama, S. Saito, Y. Suwa, and J. Yokoyama, JCAP **0806**, 020 (2008), 0804.1827.
  - [7] S. Kuroyanagi, C. Gordon, J. Silk, and N. Sugiyama, Phys. Rev. **D81**, 083524 (2010), 0912.3683.
  - [8] R. Durrer and J. Hasenkamp, Phys.Rev. **D84**, 064027 (2011), 1105.5283.
  - [9] E. Komatsu et al. (WMAP), Astrophys. J. Suppl. **192**, 18 (2011), 1001.4538.
  - [10] G. Harry, P. Fritschel, D. Shaddock, W. Folkner, and E. Phinney, Class.Quant.Grav. **23**, 4887 (2006).
  - [11] S. Kawamura, M. Ando, N. Seto, S. Sato, T. Nakamura, et al., Class.Quant.Grav. **28**, 094011 (2011).
  - [12] N. Seto, S. Kawamura, and T. Nakamura, Phys.Rev.Lett. **87**, 221103 (2001), astro-ph/0108011.
  - [13] D. J. Schwarz, C. A. Terrero-Escalante, and A. A. Garcia, Phys. Lett. **B517**, 243 (2001), astro-ph/0106020.
  - [14] S. Kuroyanagi and T. Takahashi, JCAP **1110**, 006 (2011), 1106.3437.
  - [15] S. M. Leach and A. R. Liddle, Phys. Rev. **D63**, 043508 (2001), astro-ph/0010082.
  - [16] H. Peiris and R. Easther, JCAP **0610**, 017 (2006), astro-ph/0609003.
  - [17] R. Bean, X. Chen, H. V. Peiris, and J. Xu, Phys. Rev. **D77**, 023527 (2008), 0710.1812.
  - [18] L. Lorenz, J. Martin, and C. Ringeval, Phys. Rev. **D78**, 063543 (2008), 0807.2414.
  - [19] F. Finelli, J. Hamann, S. M. Leach, and J. Lesgourgues (2009), 0912.0522.
  - [20] M. J. Mortonson, H. V. Peiris, and R. Easther, Phys. Rev. **D83**, 043505 (2011), 1007.4205.
  - [21] J. Martin, C. Ringeval, and R. Trotta, Phys.Rev. **D83**, 063524 (2011), 1009.4157.
  - [22] D. Larson et al., Astrophys. J. Suppl. **192**, 16 (2011), 1001.4635.
  - [23] N. Jarosik et al., Astrophys. J. Suppl. **192**, 14 (2011), 1001.4744.
  - [24] A. G. Riess et al., Astrophys. J. **699**, 539 (2009), 0905.0695.
  - [25] M. Maggiore, Phys.Rept. **331**, 283 (2000), gr-qc/9909001.
  - [26] S. Kuroyanagi, T. Chiba, and N. Sugiyama, Phys.Rev. **D83**, 043514 (2011), 1010.5246.
  - [27] M. S. Turner, M. J. White, and J. E. Lidsey, Phys.Rev. **D48**, 4613 (1993), astro-ph/9306029.
  - [28] M. S. Turner, Phys. Rev. **D28**, 1243 (1983).
  - [29] M. Zaldarriaga, D. N. Spergel, and U. Seljak, Astrophys.J. **488**, 1 (1997), astro-ph/9702157.
  - [30] N. Seto, Phys.Rev. **D73**, 063001 (2006), gr-qc/0510067.
  - [31] T. P. Collaboration (Planck) (2006), astro-ph/0604069.
  - [32] D. Baumann et al. (CMBPol Study Team), AIP Conf.Proc. **1141**, 10 (2009), 0811.3919.
  - [33] J. R. Bond, G. Efsthathiou, and M. Tegmark, Mon. Not. R. Astron. Soc. **291**, L33 (1997), arXiv:astro-ph/9702100.
  - [34] V. Corbin and N. J. Cornish, Class.Quant.Grav. **23**, 2435 (2006), gr-qc/0512039.
  - [35] C. Cutler and J. Harms, Phys. Rev. **D73**, 042001 (2006), gr-qc/0511092.
  - [36] J. Harms, C. Mahrtdt, M. Otto, and M. Priess, Phys. Rev. **D77**, 123010 (2008), 0803.0226.
  - [37] K. Yagi and N. Seto, Phys. Rev. **D83**, 044011 (2011), 1101.3940.
  - [38] A. Kosowsky, M. S. Turner, and R. Watkins, Phys.Rev.Lett. **69**, 2026 (1992).
  - [39] A. Kosowsky, M. S. Turner, and R. Watkins, Phys.Rev. **D45**, 4514 (1992).

- [40] M. Kamionkowski, A. Kosowsky, and M. S. Turner, Phys.Rev. **D49**, 2837 (1994), astro-ph/9310044.
- [41] C. Caprini, R. Durrer, and G. Servant, Phys.Rev. **D77**, 124015 (2008), 0711.2593.
- [42] C. Caprini, R. Durrer, and G. Servant, JCAP **0912**, 024 (2009), 0909.0622.
- [43] S. Khlebnikov and I. Tkachev, Phys.Rev. **D56**, 653 (1997), hep-ph/9701423.
- [44] R. Easther and E. A. Lim, JCAP **0604**, 010 (2006), astro-ph/0601617.
- [45] J. Garcia-Bellido and D. G. Figueroa, Phys.Rev.Lett. **98**, 061302 (2007), astro-ph/0701014.
- [46] J. Garcia-Bellido, D. G. Figueroa, and A. Sastre, Phys.Rev. **D77**, 043517 (2008), 0707.0839.
- [47] J. F. Dufaux, A. Bergman, G. N. Felder, L. Kofman, and J.-P. Uzan, Phys.Rev. **D76**, 123517 (2007), 0707.0875.
- [48] N. Barnaby, J. Moxon, R. Namba, M. Peloso, G. Shiu, et al., Phys.Rev. **D86**, 103508 (2012), 1206.6117.
- [49] A. Vilenkin, Phys.Lett. **B107**, 47 (1981).
- [50] C. Hogan and M. Rees, Nature **311**, 109 (1984).
- [51] T. Vachaspati and A. Vilenkin, Phys.Rev. **D31**, 3052 (1985).
- [52] T. Damour and A. Vilenkin, Phys.Rev. **D64**, 064008 (2001), gr-qc/0104026.
- [53] S. Olmez, V. Mandic, and X. Siemens, Phys.Rev. **D81**, 104028 (2010), 1004.0890.
- [54] H. Kudoh, A. Taruya, T. Hiramatsu, and Y. Himemoto, Phys. Rev. **D73**, 064006 (2006), gr-qc/0511145.
- [55] S. Kuroyanagi, K. Nakayama, and S. Saito, Phys.Rev. **D84**, 123513 (2011), 21 pages, 8 figures, 1110.4169.